

Detecting Axion-Like Particles with Primordial Black Holes

Kaustubh Agashe,^{1,*} Jae Hyeok Chang,^{1,2,†} Steven J. Clark,^{3,4,5,‡}
Bhaskar Dutta,^{6,§} Yuhsin Tsai,^{7,¶} and Tao Xu^{8,9,**}

¹*Maryland Center for Fundamental Physics, Department of Physics,
University of Maryland, College Park, MD 20742, USA*

²*Department of Physics and Astronomy, Johns Hopkins University, Baltimore, MD 21218, USA*

³*Department of Physics, Brown University, Providence, RI 02912-1843, USA*

⁴*Brown Theoretical Physics Center, Brown University, Providence, RI 02912-1843, USA*

⁵*Hood College, Frederick, MD 21701, USA*

⁶*Mitchell Institute for Fundamental Physics and Astronomy,
Department of Physics and Astronomy, Texas A&M University, College Station, TX 77845, USA*

⁷*Department of Physics, University of Notre Dame, IN 46556, USA*

⁸*Department of Physics and Astronomy, University of Oklahoma, Norman, OK 73019, USA*

⁹*Racah Institute of Physics, Hebrew University of Jerusalem, Jerusalem 91904, Israel*

Future gamma-ray experiments, such as the e-ASTROGAM and AMEGO telescopes, can detect the Hawking radiation of photons from primordial black holes (PBHs) if they make up a fraction or all of dark matter. PBHs can analogously also Hawking radiate new particles, which is especially interesting if these particles are mostly secluded from the Standard Model (SM) sector, since they might therefore be less accessible otherwise. A well-motivated example of this type is axion-like particles (ALPs) with a tiny coupling to photons. We assume that the ALPs produced by PBHs decay into photons well before reaching the earth, so these will augment the photons directly radiated by the PBHs. Remarkably, we find that the peaks in the energy distributions of ALPs produced from PBHs are different than the corresponding ones for Hawking radiated photons due to the spin-dependent greybody factor. Therefore, we demonstrate that this process will in fact distinctively modify the PBHs' gamma-ray spectrum relative to the SM prediction. We use monochromatic asteroid-mass PBHs as an example to show that e-ASTROGAM can observe the PBH-produced ALP gamma-ray signal (for masses up to ~ 60 MeV) and further distinguish it from Hawking radiation without ALPs. By measuring the gamma-ray signals, e-ASTROGAM can thereby probe yet unexplored parameters in the ALP mass and photon coupling.

I. INTRODUCTION

Future satellite telescopes, like the proposed e-ASTROGAM [1] and AMEGO [2] experiments, will play a vital role in multimessenger astrophysics and cover the energy gap in the current gamma-ray observations between order 0.1 to 10 MeV scales. This energy window includes motivated target signals from beyond the Standard Model (BSM) physics, such as the gamma-rays produced from dark matter (DM) annihilation [3–9], from the Hawking radiation of primordial black holes (PBHs) [9–13], or from the decay of axion-like particles (ALPs) produced in the early universe [13]. If more than one type of BSM physics exists in nature, the new physics objects can also couple to each other through SM or BSM interactions, or at a minimum via gravity. A careful measurement of the gamma-ray spectrum in these experiments may simultaneously identify signals with more than one BSM origin.

In this work, we investigate the possibility of using the e-ASTROGAM experiment to identify the Galactic Center gamma-ray signal from PBHs. The signal is composed of both direct PBH production of photons and indirect production from ALPs Hawking radiated by the PBHs. These ALPs subsequently decay into photons well before reaching the earth, producing the indirect secondary signal. In particular, we study the Hawking radiation of PBHs with asteroid-scale mass $M_{\text{PBH}} \sim 10^{15-17}$ g that emit with Hawking temperatures $T_H \approx (10^{16} \text{g}/M_{\text{PBH}}) \text{ MeV} \sim \mathcal{O}(0.1 - 10) \text{ MeV}$ and have a lifetime $\tau \approx 10^5 (M_{\text{PBH}}/10^{16} \text{g})^3 \text{ Gyrs}$ comparable to the age of the universe if $M_{\text{PBH}} \lesssim 10^{15} \text{ g}$. We map out the ALP and PBH parameters for observing the galactic gamma-ray signal at e-ASTROGAM, and further discuss the possibility of distinguishing signals from PBH with and without ALP production.

Before discussing our work, we provide a quick review of the components in our analysis, starting with PBHs. The PBH has long been considered a plausible candidate for all or a fraction of cold dark matter (CDM) [14]. There are many proposals for producing PBHs in the early universe, such as a cosmological scenario that produces an order one density contrast in the early universe [15–24], first order phase transitions [25–36], the dynamics of scalar field fragmentations [37–40], and collapse of cosmic strings [41–44] or domain walls [45, 46]. Hawking radiation produces BSM particles with rates that only

*Electronic address: kagashe@umd.edu

†Electronic address: jaechang@umd.edu

‡Electronic address: sclark@hood.edu

§Electronic address: dutta@tamu.edu

¶Electronic address: ytsai3@nd.edu

**Electronic address: tao.xu@ou.edu

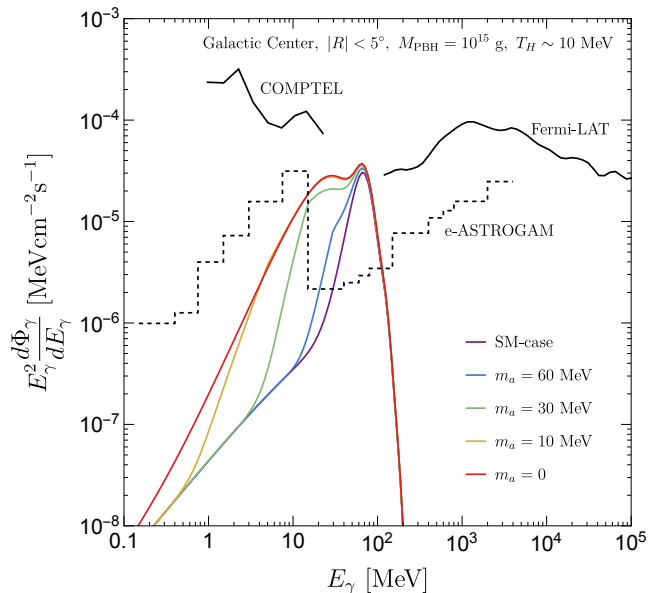


Figure 1: An example of the gamma-ray spectrum from Hawking radiation with the SM-case (Purple) and the ALP-case with $m_a = 60$ MeV (Blue), $m_a = 30$ MeV (Green), $m_a = 10$ MeV (Yellow), $m_a = 0$ MeV (Red). The PBH mass is $M_{\text{PBH}} = 10^{15}$ g, corresponding to $T_H \approx 10$ MeV, and the energy density fraction of DM is $f_{\text{PBH}} = 10^{-8}$. In this figure, we assume the ALP decay length is much shorter than the distance to the sources (PBHs) and consider its decay to be prompt (instantaneous after creation) when calculating the ALP-case flux. The ROI is chosen to be the Galactic Center with $|R| \leq 5^\circ$. Experimental constraints and future sensitivity are shown in black for COMPTEL (Solid), Fermi-LAT (Solid), and e-ASTROGAM (Dashed).

depend on particles’ masses and spins regardless of their coupling to the SM sector. Therefore, PBHs are a source for producing BSM particles even if their relic abundance is negligible. Many studies discuss the PBH production of DM or dark radiation [47–58], ALP [59–61], or the baryon asymmetry [62–74] before Big-bang Nucleosynthesis (BBN), i.e., in the relatively early universe. Our focus instead will be on the PBH production of new particles at a low redshift, so that the relevant experiments can detect PBH signals both from the SM and the BSM particles that they produce *currently*.

Previous analyses from the COMPTEL [75] and Fermi-LAT [76] experiments set upper bounds on the direct gamma-ray flux from PBHs. The better sensitivity of the e-ASTROGAM experiment opens up a new window for PBH observation between $E_\gamma \approx 0.1 - 10$ MeV and flux $E_\gamma^2 d\Phi/dE_\gamma \approx 10^{-6} - 10^{-5}$ MeVcm $^{-2}$ s $^{-1}$, which corresponds to signals from PBHs with a monochromatic asteroid-scale mass and energy density fraction f_{BH} (of the total DM density) that satisfies $10^{-6} \lesssim f_{\text{PBH}}(10^{16} \text{ g}/M_{\text{PBH}})^3 \lesssim 10^{-4}$ [10].

In this work, we extend the target for the gamma-ray search of BSM physics from PBHs alone to new particles

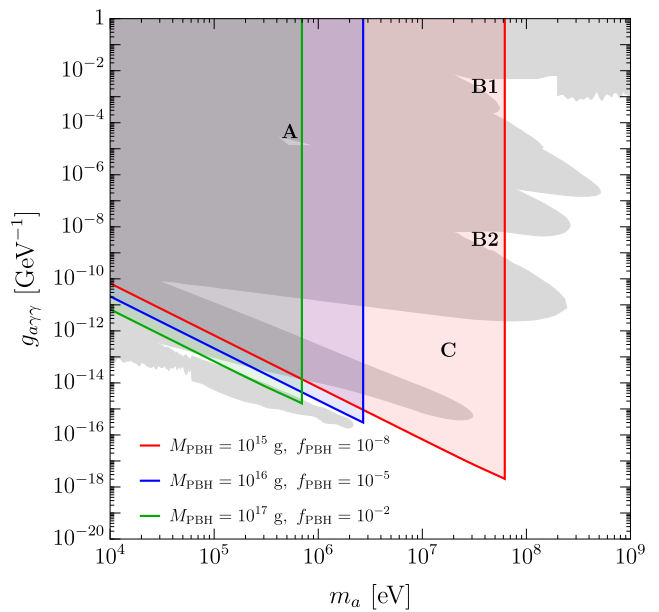


Figure 2: The ALP parameter space that can be probed by PBHs. The PBH parameters are chosen as $M_{\text{PBH}} = 10^{15}$ g, $f_{\text{PBH}} = 10^{-8}$ (Red); $M_{\text{PBH}} = 10^{16}$ g, $f_{\text{PBH}} = 10^{-5}$ (Blue); $M_{\text{PBH}} = 10^{17}$ g, $f_{\text{PBH}} = 10^{-2}$ (Green). Existing bounds (Grey) are taken from [96–108].

produced by the PBHs, focusing on ALPs as an illustration. Namely, we study the signal in the “ALP-case”, which refers to the PBH scenario that produces ALPs from Hawking radiation, followed by their prompt decay into photons, thus modulating the direct photon production by PBHs. Then, we compare the signal to the “SM-case”, which refers to the PBH scenarios with only SM particles. Because the observation of the galactic gamma-ray signal sets a stronger bound on the PBH abundance than the search of dwarf spheroidal galaxies [10], we focus on the Milky Way galactic signal for the ALP-case.

ALPs are a widely studied subject in particle physics and cosmology, where the axion field was originally proposed to solve the strong CP problem in QCD [77, 78] and later realized to be a viable DM candidate [79–82]. The ALP generalizes the phenomenology of the QCD axion without a necessary connection to the strong CP problem, but it can help to address other physics questions such as cosmic inflation [83–85], hierarchy problems [86–88], or serve as a benchmark target for DM searches [89–92]. Some earlier experiments and astrophysical and cosmological studies have also excluded part of the parameter space for the axion mass and coupling, see [93–95] for recent reviews. If the ALP is indeed responsible for one of the physics puzzles described above, the existence of PBHs guarantees ALP production when the process is kinetically allowed. We consider the ALP scenario with the Lagrangian

$$\mathcal{L}_{a\gamma\gamma} \supset \frac{1}{2} \partial_\mu a \partial^\mu a - \frac{1}{2} m_a^2 a^2 + \frac{g_{a\gamma\gamma}}{4} a F_{\mu\nu} \tilde{F}^{\mu\nu}. \quad (1)$$

The ALP can decay into two photons with the $aF_{\mu\nu}\tilde{F}^{\mu\nu}$ coupling. Here we assume the di-photon channel dominates the ALP decay for the mass $m_a < 100$ MeV¹ considered in this work. This assumption is realized in axion models where the SM leptons do not carry the Peccei-Quinn (PQ) charge, such as the well-studied KSVZ model where axion couples to SM through heavy vector-like quarks [109, 110]. In this case, the ALP decay width in the rest frame is

$$\Gamma_a = \frac{g_{a\gamma\gamma}^2 m_a^3}{64\pi}. \quad (2)$$

We can then summarize our results of working out the “interaction” between PBHs and ALPs as follows. Since PBHs produce ALPs with a nearly thermal energy distribution E_a , after traveling distance D from the PBH, the produced ALPs decay into photons with a probability

$$P_{a,\text{decay}}(E_a, D) = 1 - \exp\left(-D \Gamma_a \frac{m_a}{\sqrt{E_a^2 - m_a^2}}\right). \quad (3)$$

The ALP-case, therefore, has a gamma-ray spectrum both from the direct PBH production and a secondary emission from the ALP decay. In Fig. 1, we show the photon spectrum in the ALP-case for $M_{\text{PBH}} = 10^{15}$ g, $f_{\text{PBH}} = 10^{-8}$, and different ALP masses. In the example, the Hawking temperature $T_H \approx 10$ MeV generates a primary gamma-ray spectrum peaked around $10 T_H$ [111]. In general, due to the spin-0 greybody factor, $E_\gamma < E_a$ from the ALP decay, and the suppressed production of ALPs much heavier than the primary photon peak, the visible ALP peak is always on the left side of the primary peak. The ALP spectrum has a different peak location and spectral shape than the photon spectrum in the SM-case, and the double-peak feature of the spectral shape makes it possible to distinguish between the signals for the ALP- and SM-cases. We leave the details of the spectrum calculation to Sec. II.

For claiming the observation of the ALP signal, since we do not know *a priori* the PBH mass and abundance, we need to be able to distinguish the photon spectrum in Fig. 1 from the SM-case with arbitrary PBH parameters. We conduct a less ambitious study in this work by assuming PBH with a monochromatic mass spectrum. With the expected e-ASTROGAM sensitivity given in [2], we calculate the region of m_a and f_{PBH} for a given M_{PBH} that allows the e-ASTROGAM to differentiate signals in the ALP-case from the SM-case.

Fig. 2 summarizes regions of the ALP parameters we identify that allow 3σ e-ASTROGAM differentiation between the ALP- and SM-case signals. The lower boundaries of each colored region give the minimum $g_{a\gamma\gamma}$ for

ALPs produced at Galactic Center from PBH to have $P_{a,\text{decay}} = 0.99$ decay before reaching the earth. We consider the E_a distribution from the Hawking radiation in the probability calculation described in Sec. II. The right boundary of each colored region indicates the maximum ALP mass that can be produced and generate distinct enough signals between the two cases. We explain the details of the calculation in Sec. III.

Fig. 2 also shows the existing exclusion bounds (light grey) from various collider, astrophysical, and cosmological analyses. To enlarge the allowed ALP parameter space for the indirect detection signal, we already assume a low reheating temperature $T_{\text{reh}} = 5$ MeV that weakens the BBN+ ΔN_{eff} bound [107, 108]. Our result shows three regions of the ALP parameter space for identifying the ALP-case signals. Parameters around the so-called cosmological triangle region at point **A** can exist either with the presence of ΔN_{eff} , a non-vanishing neutrino chemical potential, or a lower reheating temperature [112, 113]². For PBH mass around 10^{15} g, the corresponding Hawking temperature is high enough to produce ALPs with $m_a \approx 10 - 60$ MeV. The ALPs in the region around **B1** and **B2** permit distinctive enough gamma-ray signals compared to the SM-case. However, the ALPs need to have dominant decay into photons even if the $a \rightarrow e^+e^-$ decay is kinematically allowed. As mentioned above, the dominant photon decay can be achieved in models like the KSVZ scenario where the SM leptons do not carry the PQ charge. The allowed parameter space in the **C** region remains open for the ALP-case signal if the universe has a low reheating temperature ≈ 5 MeV. A higher reheating temperature can thermally produce relativistic ALPs and therefore generate ΔN_{eff} that violates the BBN constraint. For the following study, we assume the ALP with a given m_a has a value of $g_{a\gamma\gamma}$ that is outside of the excluded (grey) region but inside the colored (green, blue, red) region (making the signal observable) and will not specify the coupling again.

The format of the paper is as follows. In Sec. II, we review the calculation of gamma-ray and ALP production from Hawking radiation. We calculate the galactic gamma-ray signal from the ALP-case by including the proper J -factor integral. In Sec. III, we conduct a likelihood analysis for distinguishing the ALP-case signal from the SM-case signal. We conclude in Sec. IV.

¹ For the PBH masses we consider, ALPs with $m_a > 100$ MeV have negligible production rates. For $m_a < 100$ MeV $< 2m_\pi$, decay into SM hadrons is kinematically forbidden.

² Ref. [114] shows the possibility of excluding the cosmological triangle region from the estimate of the supernovae explosion energy. However, the argument relies on certain assumptions of the proto-neutron star model, and the bound can be weakened with a different assumption of the proto-neutron star property.

II. HAWKING RADIATION FROM PRIMORDIAL BLACK HOLES

A black hole is expected to emit particles constantly near its event horizon, and this phenomenon is called Hawking radiation [115]. In this section, we review particle spectra of Hawking radiation, mostly following [10]. Particles directly produced from black holes are called primary particles, while particles from the result of interactions of primary particles are called secondary particles. The number of produced primary particle i per unit time per unit energy from a black hole with mass M is given by [115–117]

$$\frac{\partial N_{i,\text{primary}}}{\partial E_i \partial t} = \frac{g_i}{2\pi} \frac{\Gamma_i(E_i, M, \mu_i)}{e^{E_i/T_H} \pm 1}, \quad (4)$$

where μ_i and g_i are the mass and the degree of freedom of particle i , Γ_i is the greybody factor, $T_H = 1/(8\pi GM)$ is the Hawking temperature, and the plus and minus signs correspond to whether the produced particle is a fermion or a boson, respectively. The spin-dependant greybody factor approaches the geometrical optics limit $\Gamma_i = 27G^2 M^2 E_i^2$ for high energies. We use **Black-Hawk** package [118, 119] to get the grey body factor Γ_i . The particle rest mass cuts the evaporation spectrum to $E_i \geq \mu_i$.

We are interested in the photon spectrum of Hawking radiation, which includes the primary spectrum and the secondary spectrum from decay and final state radiation (FSR) of primary particles.

$$\begin{aligned} \frac{\partial N_{\gamma,\text{tot}}}{\partial E_\gamma \partial t} &= \frac{\partial N_{\gamma,\text{primary}}}{\partial E_\gamma \partial t} \\ &+ \sum_{i=\pi^0, a} \int dE_i 2 \frac{\partial N_{i,\text{primary}}}{\partial E_i \partial t} \frac{dN_{i,\text{decay}}}{dE_\gamma} \\ &+ \sum_{i=e^\pm, \mu^\pm, \pi^\pm} \int dE_i \frac{\partial N_{i,\text{primary}}}{\partial E_i \partial t} \frac{dN_{i,\text{FSR}}}{dE_\gamma} \end{aligned} \quad (5)$$

with

$$\frac{dN_{i,\text{decay}}}{dE_\gamma} = \frac{\Theta(E_\gamma - E_i^-) \Theta(E_i^+ - E_\gamma)}{E_i^+ - E_i^-} \quad (6)$$

$$E_i^\pm = \frac{1}{2} \left(E_i \pm \sqrt{E_i^2 - m_i^2} \right) \quad (7)$$

$$\frac{dN_{i,\text{FSR}}}{dE_\gamma} = \frac{\alpha}{\pi Q_i} P_{i \rightarrow i\gamma}(x) \left[\log \left(\frac{1-x}{\mu_i^2} \right) - 1 \right] \quad (8)$$

$$P_{i \rightarrow i\gamma}(x) = \begin{cases} \frac{2(1-x)}{x}, & i = \pi^\pm \\ \frac{1+(1-x)^2}{x}, & i = \mu^\pm, e^\pm \end{cases} \quad (9)$$

Note we ignore the three-body decay from μ^\pm and π^\pm . These processes are safe to be ignored because they are much heavier than the energy range we are interested.

The greybody factor for scalar particles has a peak at a smaller energy compared to vectors; the ALP-case spectrum has a ‘‘double peak’’ feature as shown in Fig. 1, and this is distinguishable from the SM-case spectrum.

The photon flux near the Earth is

$$\frac{d\Phi_\gamma}{dE_\gamma} = \bar{J}_D \frac{\Delta\Omega}{4\pi} \int dM \frac{f_{\text{PBH}}(M)}{M} \frac{\partial N_{\gamma,\text{tot}}}{\partial E_\gamma \partial t}. \quad (10)$$

\bar{J}_D is the so-called J-factor for decay, which is given by

$$\bar{J}_D = \frac{1}{\Delta\Omega} \int_{\Delta\Omega} d\Omega \int_{\text{LOS}} dl \rho_{\text{DM}}. \quad (11)$$

To get the J-factor, we assume the DM distribution in the Milky-Way halo follows a Navarro–Frenk–White (NFW) profile [120]

$$\rho_{\text{DM}}(r) = \frac{\rho_s}{\frac{r}{r_s} (1 + \frac{r}{r_s})^2} \Theta(r_{200} - r). \quad (12)$$

We use $r_s = 11$ kpc, $\rho_s = 0.838$ GeV/cm³, $r_{200} = 193$ kpc and $r_\odot = 8.122$ kpc [121]. For our ROI of $|R| < 5^\circ$ from the Galactic Center, the J-factor is $\bar{J}_D = 1.597 \times 10^{26}$ MeVcm⁻²sr⁻¹ and the angular size is $\Delta\Omega = 2.39 \times 10^{-2}$ sr.

In this study, we assume the PBH mass distribution is monochromatic, which can be produced from, for example, the collapse of Q-balls [122] or first-order phase transition [123]. Taking $f_{\text{PBH}}(M) = f_{\text{PBH}} \delta(M - M_{\text{PBH}})$, Eq. (10) simplifies to

$$\frac{d\Phi_\gamma}{dE_\gamma} = \bar{J}_D \frac{\Delta\Omega}{4\pi} \frac{f_{\text{PBH}}}{M_{\text{PBH}}} \frac{\partial N_{\gamma,\text{tot}}}{\partial E_\gamma \partial t} \quad (13)$$

In order for ALPs to change the photon spectrum near the earth, they must decay before reaching the earth. The decay probability of ALPs while propagating to the earth from Galactic Center with a monochromatic PBH mass is given by

$$\langle P_{a,\text{decay}} \rangle \equiv \frac{\Phi_{a,\text{dec}}}{\Phi_{a,\text{tot}}}, \quad (14)$$

where

$$\Phi_{a,\text{tot}} = \int_{\Delta\Omega} \frac{d\Omega}{4\pi} \int_{\text{LOS}} d\ell \int dE_a \frac{f_{\text{PBH}} \rho_{\text{DM}}}{M_{\text{PBH}}} \frac{\partial N_{a,\text{primary}}}{\partial E_a \partial t} = \bar{J}_D \frac{\Delta\Omega}{4\pi} \frac{f_{\text{PBH}}}{M_{\text{PBH}}} \int dE_a \frac{\partial N_{a,\text{primary}}}{\partial E_a \partial t}, \quad (15)$$

$$\Phi_{a,\text{dec}} = \int_{\Delta\Omega} \frac{d\Omega}{4\pi} \int_{\text{LOS}} d\ell \int dE_a \frac{f_{\text{PBH}} \rho_{\text{DM}}}{M_{\text{PBH}}} \frac{\partial N_{a,\text{primary}}}{\partial E_a \partial t} P_{a,\text{decay}}(E_a, \ell), \quad (16)$$

and $P_{a,\text{decay}}$ is given by Eq. (3). We require $\langle P_{a,\text{decay}} \rangle$ larger than 99% to get the lower boundaries of the color curves in Fig. 2. For most of the parameter regions shown in Fig. 2, we can assume the ALP decay is prompt as $g_{a\gamma\gamma}$ is at least one order of magnitude larger than the lower boundaries. Since the ALP decay width is proportional to the square of the coupling $\Gamma_a \propto g_{a\gamma\gamma}^2$, even the decay length of ALPs in region C is much smaller than the distance between the earth and Galactic Center.

III. EXPERIMENTS AND LIKELIHOOD ANALYSIS

In order to place constraints on individual models, we use the likelihood analysis outlined in [111]. In this analysis, an assumption is made about a “true” model that produces an observational gamma-ray signal. A test model is also chosen for comparison. The likelihood that the test model will replicate the gamma-ray signal produced by the true model follows Poisson statistics and is expressed as

$$\mathcal{L} = \exp\left(\sum_i n_i \ln \sigma_i - \sigma_i - \ln n_i!\right) \quad (17)$$

where n_i is the photon count of the true model (including any additional background signals) and σ_i is the expected photon count from the test model (including background) in the i -th energy bin. For comparison of different models, we utilize the test statistic (TS)

$$\text{TS} = -2 \ln \left(\frac{\mathcal{L}}{\mathcal{L}_{\text{true}}} \right) = \Sigma^2, \quad (18)$$

where Σ is the observational significance [124–127] and $\mathcal{L}_{\text{true}}$ is the likelihood of the true model. Here, we are assuming that the joint analysis of the gamma-ray energy bins follows a χ^2 distribution, and unless otherwise stated, we take $\Sigma = 3$. In order to reduce complexity and statistical fluctuations in the likelihood determination, we also take the true signal as its statistical mean.

In creating the true and test signals as well as the expected background, we use the 5° NFW Galactic Center as the source for the observational signal (see Sec. II) and use estimations of the e-ASTROGAM detector sensitivities and specifications as well as the forecasted astrophysical background [1, 111]. Please refer to Ref. [111] for more details about the detector sensitivity and foreground used.

A. Signal Detection and Distinguishability between SM and ALP

In order to determine whether a particular model is observable, we perform the analysis described above using the background as the “true” model. The parameter space of the test model is then scanned over in order to determine the parameter values such that the likelihood differs by a specified significance.³ These results correspond to the PBH discovery bounds in Fig. 4. If the population of PBH is above the corresponding line, then the PBH will be bright enough that they are distinguishable from the background. Note that for a particular M_{PBH} and m_a , the ALP-case bound is always equal to or stronger than the SM-case bound. This is due to the PBHs producing the same SM particles; however, with the introduction of ALPs, there is an additional degree of freedom which results in a brighter, thus easier to observe, signal. Also note that for heavier PBHs or heavier ALPs, the ALP-case asymptotes to the SM-case. This is due to the ALP degree of freedom becoming exponentially suppressed when the Hawking temperature is much lower than m_a .

In addition to determining the point at which a given signal is observable, it is also convenient to discuss the parameter space where the ALP-case is distinguishable from the SM-case. To illustrate this, Fig. 3 shows 3σ contours from e-ASTROGAM constraining the PBH parameter space using Galactic Center data assuming that the underlying “true” model is the ALP-case with $m_a = 10^{-1}$ MeV, $M_{\text{PBH}} = 10^{16}$ g, and with various $f = f_{\text{PBH, true}}$. The y -axis corresponds to the ratio between the test PBH fraction, $f_{\text{PBH, test}}$, and $f_{\text{PBH, true}}$.⁴ As $f_{\text{PBH, true}}$ increases, the signal-to-noise ratio also increases, thus strengthening the observability of the signal and the constraining capabilities of an experiment. In Fig. 3, the “ \star ” indicates the location of the “true” model.

³ During the scan, we assume that the likelihood always decreases with increasing f_{PBH} .

⁴ The ratio was chosen for display purposes so that the true model is a fixed point in the figure rather than drifting. This has the additional benefit that no constraining curves intersect, but the disadvantage is that the upper boundaries (when there is insufficient signal to make any observation) become separate lines instead of a single result representing an upper bound on the parameter space.

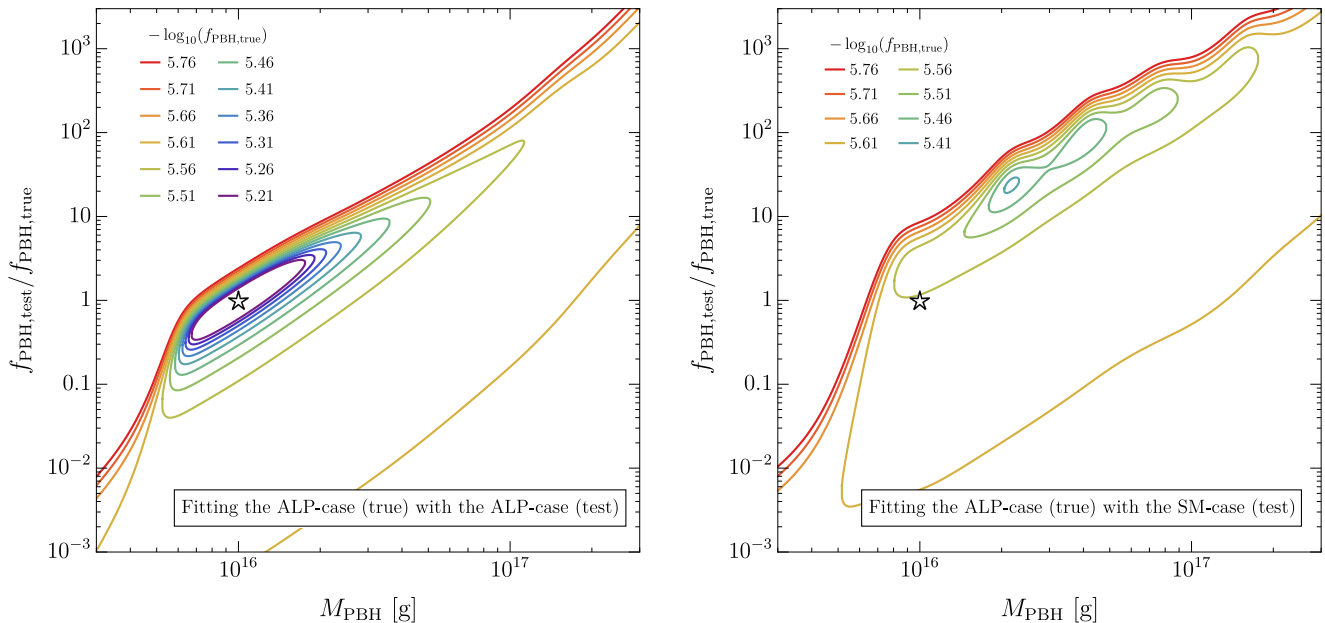


Figure 3: The 3σ contours from the Galactic Center constraining the PBH parameter space, assuming that the underlying “true” model is the ALP-case with $m_a = 10^{-1}$ MeV, $M_{\text{PBH}} = 10^{16}$ g, and various $f_{\text{PBH, true}}$. The “test” models are (*left*) the ALP-case and (*right*) the SM-case. The “ \star ” indicates the location of the true model. With increasing $f_{\text{PBH, true}}$, the contours shrink. When the test model matches the true model (as is the case in the left panel), the contours become infinitesimally small, while for a mismatched model (*right*), they eventually disappear with sufficient data such that no contour may be drawn. We define the values of $f_{\text{PBH, true}}$ where the contour disappears in the right panel as “identification of ALP” line in Fig. 4. The values of $f_{\text{PBH, true}}$ for contours are shown in each plot.

The two panels correspond to constraining the observation with the same model (*left*: ALP-case) and a different model (*right*: SM-case). The contours indicate the region of parameter space inside which can replicate the observational signal at the desired confidence. If the signal is too insufficient, only upper bounds can be placed. This is observed in the figure by the un-closed contours. As $f_{\text{PBH, true}}$ increases, the signal increases and eventually lower bounds can be placed, as indicated by the closing of the contours. With further increases to $f_{\text{PBH, true}}$, the contours shrink. If the test model matches the true model, the contours continuously shrink and eventually become infinitesimally small as the parameters of the true model are precisely determined (*left*). However, if the test model does not match, the contours will eventually collapse (no contours exist for $-\log_{10}(f_{\text{PBH, true}}) \leq 5.40$) and no model parameter values will be able to replicate the signal (*right*). Note that these contours do not refer to those for constraining a particular PBH signal over the background, but rather the capability to confine PBH parameters given a particular observation. In order for a model to be distinguishable from another, the parameter space of one of the models must completely disappear. We utilize this behavior by assuming that there is a PBH signal (the chosen underlying model is the ALP-case) and scan over models where PBH only produce the SM-case. In the scan, we search for the value of $f_{\text{PBH, true}}$ where the

SM-case parameter space completely disappears. This is equivalent to searching for the parameter values where the likelihood of the bestfit model is equal to the significance criteria.⁵

We are therefore able to define the f_{PBH} for a given M_{PBH} and m_a where the ALP-case is discernible from SM-case. This value of f_{PBH} is the black hole fraction needed for the allowable SM-case PBH parameter space to completely disappear at a given confidence interval. This discernability threshold is shown in Fig. 4 for various M_{PBH} (*left*) and m_a (*right*) with the other parameter fixed.

In the M_{PBH} plane of Fig. 4, all parameter values above the solid curves correspond to the region where a ALP-case signal can be distinguished from the SM-case. Also included are the corresponding lower limits for f_{PBH} in order to distinguish a PBH signal from the

⁵ In this scan, it was assumed that the likelihood was single-peaked in both M_{PBH} and f_{PBH} . As observed in Fig. 3, this may not be the case; however, tests indicate that it would usually only lead to minor fluctuations in the final result. The oscillating behavior observed in the low signal-to-noise regions of Fig. 3 ultimately produces these islands as the parameter space is squeezed as it is constrained. This wave-like behavior appears to be a result of the photon energy binning and can be reduced by increased experimental resolution to allow for finer bins.

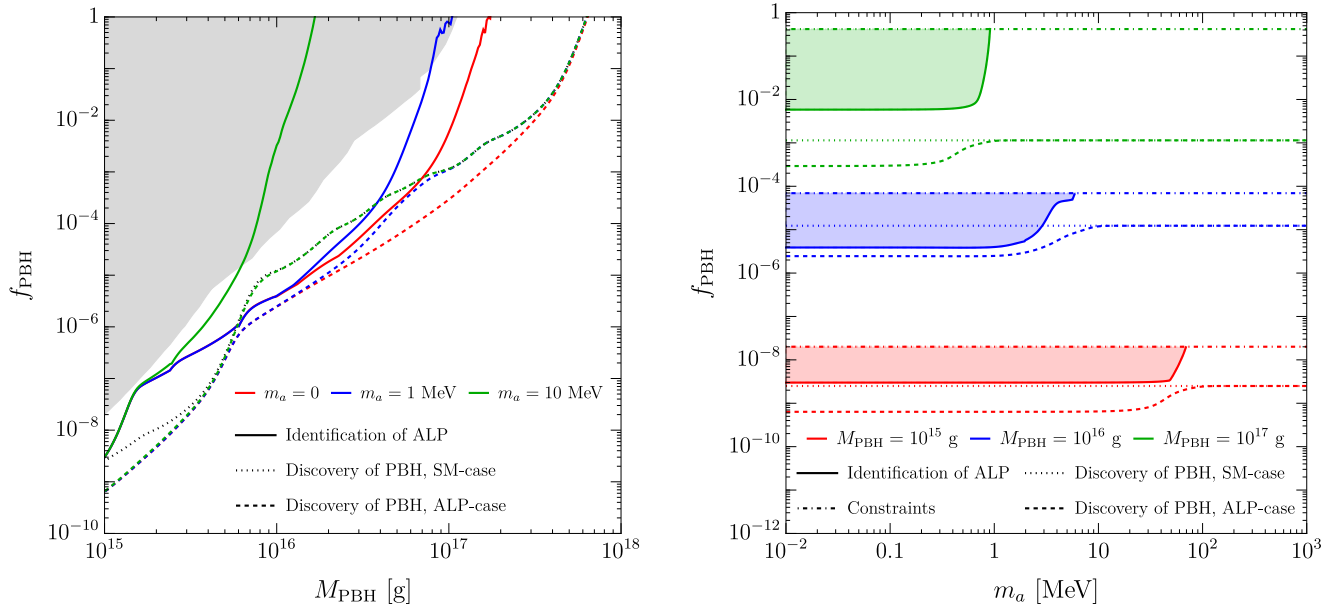


Figure 4: PBH differentiability bounds in the f_{PBH} vs M_{PBH} (left) and f_{PBH} vs m_a (right) planes. Various curves correspond to the capability to distinguish a PBH signal with the SM-case (*short-dash*) and the ALP-case (*long-dash*) from the background. Also included are the the ALP-case vs SM-case distinguishability (*solid*) and past experimental constraints (left: *shaded grey* and right: *dot-dashed*). In the m_a plane, the shaded region highlights the region that can distinguish an ALP-case signal from an SM-case signal with the far right edge corresponding to the maximum m_a allowed.

background for the ALP-case (*long dash*) and the SM-case (*short dash*). As expected, the ALP-case vs SM-case distinguishability line is always higher than the ALP-case identification line as it must first be observable before more information can be extracted. In addition, the ALP-case identification line is always beneath the SM-case identification line. This is because it is a brighter signal as mentioned previously. Other features of note are that the ALP-case and the SM-case identification lines merge for large M_{PBH} ; this is because the ALPs become exponentially suppressed as the Hawking temperature drops below their mass. This transition is also one of the causes for the distinguishability lines rapidly losing sensitivity as the ALP-case and the SM-case signals become nearly identical. The other cause is related to the experimental sensitivity as signal either leaves the detector's range (such as with high PBH masses) or enters regions of low sensitivity (the convergence of discovery lines near 5×10^{15} g are a result of the extra ALP decay photons residing in a region of low detector sensitivity). Also included are current PBH bounds for the SM-case [10, 128, 129].⁶

In the m_a plane of Fig. 4, each line style corresponds to the same result as in the f_{PBH} panel. Both the ALP-

case vs SM-case distinguishability curves (*solid*) and the ALP-case PBH background discovery curves (*long dash*) are flat for small m_a as they are essentially massless when compared with their energies. For large masses, the reverse is true and they are both nonrelativistic and exponentially suppressed as the Hawking temperature drops below their mass. This leads to another flat region for the identification from background curve as it plateaus and becomes identical to the SM-case identification curve (*short dash*). On the other hand, the ALP-case vs SM-case distinguishability curve rapidly increases due to the lack of distinguishing features. In addition, current SM-case PBH constraints are also plotted (*dot-dashed*), above which SM-case PBHs have already been constrained. The shaded regions correspond to the allowed parameter space for distinguishing the ALP-case from the SM-case, and the rightmost edge is the high m_a bound of the regions shown in Fig. 1.

IV. CONCLUSIONS AND OUTLOOK

PBHs are a plausible candidate for a fraction or all of the observed DM density. They are also a unique source for producing BSM particles, even if the new particles have a tiny coupling to the SM sector. In this work, we discuss the possibility of observing Galactic Center gamma-ray signals both from direct PBH radiation and from the decay of ALPs produced by PBHs. Under the assumption of monochromatic PBH mass, we

⁶ While these bounds will change with the introduction of the ALP, the alteration is expected not to be larger than a factor of 2 (corresponding to the massless case) due to the ALPs simply adding an additional degree of freedom.

show that with $M_{\text{PBH}} = 10^{15-17}$ g, and $m_a \lesssim 60$ MeV, e-ASTROGAM has a chance to observe both types of gamma-ray signals and distinguish the total signal from PBHs with arbitrary choices of the M_{PBH} and abundance f_{PBH} . Our findings show that future detectors such as the e-ASTROGAM and AMEGO experiments can explore both PBH and axion physics, even for ALPs that satisfies all existing constraints and have no ambient presence in the universe today. One can also consider the use of the extragalactic gamma-ray background when performing this analysis. Before considering differences in the PBH distribution and the astrophysical background, this has the potential of increasing the coverage of smaller $g_{a\gamma\gamma}$ by up to three orders of magnitude due to increasing the allowable ALP decay length to be the Horizon size. We leave this for future work.

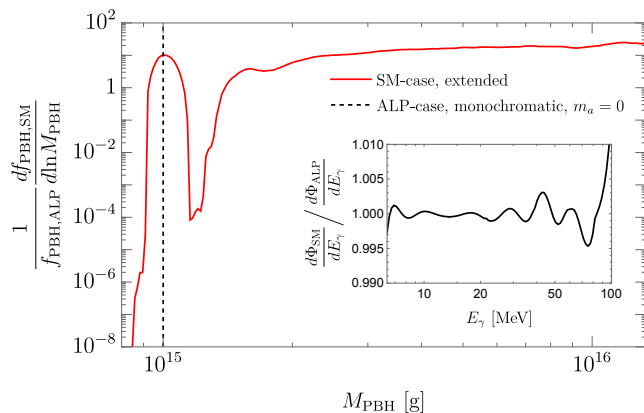


Figure 5: The extended black hole mass distribution that mimics the photon spectrum for the ALP-case with $m_a = 0$, $M_{\text{PBH}} = 10^{15}$ g, and $6 \text{ MeV} < E_\gamma < 100 \text{ MeV}$. The peak near the $M_{\text{PBH}} = 10^{15}$ g explains the primary photon peak, while the plateau at large masses is for the peak from ALP decays. To show the goodness of the fit, we show the the ratio of the gamma-ray flux between SM-case with the extended mass function and the ALP-case in the plot inside. As a result, f_{PBH} for the SM-case is more than 200 times larger than f_{PBH} for the SM-case.

To make a stronger statement in distinguishing the ALP-case signal from the SM-case, we need to perform the analysis with a more generalized PBH mass function. In this case, a non-trivial mass function may produce the “double peak” feature as in the ALP-case signal (See Fig. 1.), making it difficult to confirm the existence of the ALP decay. However, mimicking the ALP signal with an extended PBH mass function may not be trivial. Since the ALP decay mainly contributes to the softer gamma-

ray spectrum as in Fig. 1, it requires a large density of massive PBHs to fully reproduce the lower energy tail of the ALP signal. In Fig. 5, we show an example of mimicking the ALP-case signal with $M_{\text{PBH}} = 10^{15}$ g and massless ALPs by an extended PBH mass function in the SM-case. When trying to reproduce the original gamma-ray spectrum down to $E_\gamma = 6$ MeV, the plateau of the mass spectrum (red) in the higher PBH mass makes the f_{PBH} about 200 times larger than in the ALP-case. It can also be hard to realize the exotic feature of the mass spectrum that has a dip right next to the original PBH mass within the context of a cosmological model.

Even if the mass function in the SM-case mimics the ALP-case signal and satisfies the DM bound, we may use the gravitational wave (GW) signal to distinguish the ALP signal from the SM radiation. If the PBHs are produced by large primordial curvature perturbations, these will differ between the ALP-case and the SM-case which give rise to the same gamma-ray signal, since the corresponding PBH spectra are different. As studied in Ref. [111], large curvature perturbations that are associated with the production of the PBHs with the visible gamma-ray signal at e-ASTROGAM will source GW signals well above the sensitivity of future detectors. Combining the above two facts, the GW signals for the two cases will then be different, even though the gamma-ray signal is the same (the latter by design). In other words, there is a chance to distinguish the two scenarios by correlating the gamma-ray and GW signals. We leave these studies for future directions.

Note added: As we were finalizing the paper, we came to know of work by Y. Jho, T. G. Kim, J-C. Park, S-C. Park and Y. Park on a similar topic [130].

ACKNOWLEDGEMENTS

We would like to thank Henrike Fleischhack, Subhjit Ghosh, Shmuel Nussinov, and Nadav Outmezguine for useful discussions and Jong-Chul Park *et al.* for informing us about their work on a similar topic. KA and JHC were supported in part by the NSF grant PHY-2210361 and by the Maryland Center for Fundamental Physics. JHC is also supported in part by JHU Joint Postdoc Fund. BD is supported in part by DOE grant DE-SC0010813. TX is supported in part by DOE Grant desc0009956 and by the Israel Science Foundation (grant No. 1112/17). YT is supported by the NSF grant PHY-2112540.

[1] e-ASTROGAM Collaboration, A. De Angelis *et al.*, “The e-ASTROGAM mission,” *Exper. Astron.* **44** no. 1, (2017) 25–82, [arXiv:1611.02232](https://arxiv.org/abs/1611.02232)

[2] AMEGO Collaboration, R. Caputo *et al.*, “All-sky Medium Energy Gamma-ray Observatory: Exploring [\[astro-ph.HE\]](https://arxiv.org/abs/astro-ph.HE).”

- the Extreme Multimessenger Universe,” [arXiv:1907.07558 \[astro-ph.IM\]](#).
- [3] C. Boehm, T. A. Ensslin, and J. Silk, “Can Annihilating dark matter be lighter than a few GeVs?,” *J. Phys. G* **30** (2004) 279–286, [arXiv:astro-ph/0208458](#).
 - [4] J. F. Beacom, N. F. Bell, and G. Bertone, “Gamma-ray constraint on Galactic positron production by MeV dark matter,” *Phys. Rev. Lett.* **94** (2005) 171301, [arXiv:astro-ph/0409403](#).
 - [5] D. P. Finkbeiner and N. Weiner, “Exciting Dark Matter and the INTEGRAL/SPI 511 keV signal,” *Phys. Rev. D* **76** (2007) 083519, [arXiv:astro-ph/0702587](#).
 - [6] R. Essig, N. Sehgal, and L. E. Strigari, “Bounds on Cross-sections and Lifetimes for Dark Matter Annihilation and Decay into Charged Leptons from Gamma-ray Observations of Dwarf Galaxies,” *Phys. Rev. D* **80** (2009) 023506, [arXiv:0902.4750 \[hep-ph\]](#).
 - [7] R. Essig, E. Kuflik, S. D. McDermott, T. Volansky, and K. M. Zurek, “Constraining Light Dark Matter with Diffuse X-Ray and Gamma-Ray Observations,” *JHEP* **11** (2013) 193, [arXiv:1309.4091 \[hep-ph\]](#).
 - [8] K. K. Boddy and J. Kumar, “Indirect Detection of Dark Matter Using MeV-Range Gamma-Ray Telescopes,” *Phys. Rev. D* **92** no. 2, (2015) 023533, [arXiv:1504.04024 \[astro-ph.CO\]](#).
 - [9] R. Laha, J. B. Muñoz, and T. R. Slatyer, “INTEGRAL constraints on primordial black holes and particle dark matter,” *Phys. Rev. D* **101** no. 12, (2020) 123514, [arXiv:2004.00627 \[astro-ph.CO\]](#).
 - [10] A. Coogan, L. Morrison, and S. Profumo, “Direct Detection of Hawking Radiation from Asteroid-Mass Primordial Black Holes,” *Phys. Rev. Lett.* **126** no. 17, (2021) 171101, [arXiv:2010.04797 \[astro-ph.CO\]](#).
 - [11] C. Keith, D. Hooper, T. Linden, and R. Liu, “Sensitivity of future gamma-ray telescopes to primordial black holes,” *Phys. Rev. D* **106** no. 4, (2022) 043003, [arXiv:2204.05337 \[astro-ph.HE\]](#).
 - [12] X.-H. Tan, Y.-J. Yan, T. Qiu, and J.-Q. Xia, “Searching for the Signal of a Primordial Black Hole from CMB Lensing and γ -Ray Emissions,” *Astrophys. J. Lett.* **939** no. 1, (2022) L15, [arXiv:2209.15222 \[astro-ph.CO\]](#).
 - [13] A. Caputo, M. Negro, M. Regis, and M. Taoso, “Dark Matter prospects with COSI: ALPs, PBHs and sub-GeV Dark Matter,” [arXiv:2210.09310 \[hep-ph\]](#).
 - [14] B. Carr, F. Kuhnel, and M. Sandstad, “Primordial Black Holes as Dark Matter,” *Phys. Rev. D* **94** no. 8, (2016) 083504, [arXiv:1607.06077 \[astro-ph.CO\]](#).
 - [15] B. J. Carr, “The Primordial black hole mass spectrum,” *Astrophys. J.* **201** (1975) 1–19.
 - [16] P. Ivanov, P. Naselsky, and I. Novikov, “Inflation and primordial black holes as dark matter,” *Phys. Rev. D* **50** (1994) 7173–7178.
 - [17] J. Garcia-Bellido, A. D. Linde, and D. Wands, “Density perturbations and black hole formation in hybrid inflation,” *Phys. Rev. D* **54** (1996) 6040–6058, [arXiv:astro-ph/9605094](#).
 - [18] J. Silk and M. S. Turner, “Double Inflation,” *Phys. Rev. D* **35** (1987) 419.
 - [19] M. Kawasaki, N. Sugiyama, and T. Yanagida, “Primordial black hole formation in a double inflation model in supergravity,” *Phys. Rev. D* **57** (1998) 6050–6056, [arXiv:hep-ph/9710259](#).
 - [20] J. Yokoyama, “Formation of MACHO primordial black holes in inflationary cosmology,” *Astron. Astrophys.* **318** (1997) 673, [arXiv:astro-ph/9509027](#).
 - [21] S. Pi, Y.-l. Zhang, Q.-G. Huang, and M. Sasaki, “Scaloron from R^2 -gravity as a heavy field,” *JCAP* **05** (2018) 042, [arXiv:1712.09896 \[astro-ph.CO\]](#).
 - [22] M. P. Hertzberg and M. Yamada, “Primordial Black Holes from Polynomial Potentials in Single Field Inflation,” *Phys. Rev. D* **97** no. 8, (2018) 083509, [arXiv:1712.09750 \[astro-ph.CO\]](#).
 - [23] O. Özsoy, S. Parameswaran, G. Tasinato, and I. Zavala, “Mechanisms for Primordial Black Hole Production in String Theory,” *JCAP* **07** (2018) 005, [arXiv:1803.07626 \[hep-th\]](#).
 - [24] M. Cicoli, V. A. Diaz, and F. G. Pedro, “Primordial Black Holes from String Inflation,” *JCAP* **06** (2018) 034, [arXiv:1803.02837 \[hep-th\]](#).
 - [25] S. W. Hawking, I. G. Moss, and J. M. Stewart, “Bubble Collisions in the Very Early Universe,” *Phys. Rev. D* **26** (1982) 2681.
 - [26] M. Crawford and D. N. Schramm, “Spontaneous Generation of Density Perturbations in the Early Universe,” *Nature* **298** (1982) 538–540.
 - [27] H. Kodama, M. Sasaki, and K. Sato, “Abundance of Primordial Holes Produced by Cosmological First Order Phase Transition,” *Prog. Theor. Phys.* **68** (1982) 1979.
 - [28] I. G. Moss, “Black hole formation from colliding bubbles,” [arXiv:gr-qc/9405045](#).
 - [29] B. Freivogel, G. T. Horowitz, and S. Shenker, “Colliding with a crunching bubble,” *JHEP* **05** (2007) 090, [arXiv:hep-th/0703146](#).
 - [30] M. C. Johnson, H. V. Peiris, and L. Lehner, “Determining the outcome of cosmic bubble collisions in full General Relativity,” *Phys. Rev. D* **85** (2012) 083516, [arXiv:1112.4487 \[hep-th\]](#).
 - [31] A. Kusenko, M. Sasaki, S. Sugiyama, M. Takada, V. Takhistov, and E. Vitagliano, “Exploring Primordial Black Holes from the Multiverse with Optical Telescopes,” *Phys. Rev. Lett.* **125** (2020) 181304, [arXiv:2001.09160 \[astro-ph.CO\]](#).
 - [32] M. J. Baker, M. Breitbach, J. Kopp, and L. Mitnacht, “Primordial Black Holes from First-Order Cosmological Phase Transitions,” [arXiv:2105.07481 \[astro-ph.CO\]](#).
 - [33] M. J. Baker, M. Breitbach, J. Kopp, and L. Mitnacht, “Detailed Calculation of Primordial Black Hole Formation During First-Order Cosmological Phase Transitions,” [arXiv:2110.00005 \[astro-ph.CO\]](#).
 - [34] K. Kawana and K.-P. Xie, “Primordial black holes from a cosmic phase transition: The collapse of Fermi-balls,” *Phys. Lett. B* **824** (2022) 136791, [arXiv:2106.00111 \[astro-ph.CO\]](#).
 - [35] P. Huang and K.-P. Xie, “Primordial black holes from an electroweak phase transition,” *Phys. Rev. D* **105** no. 11, (2022) 115033, [arXiv:2201.07243 \[hep-ph\]](#).
 - [36] P. Lu, K. Kawana, and K.-P. Xie, “Old phase remnants in first-order phase transitions,” *Phys. Rev. D* **105** no. 12, (2022) 123503, [arXiv:2202.03439 \[astro-ph.CO\]](#).
 - [37] E. Cotner and A. Kusenko, “Primordial black holes from supersymmetry in the early universe,” *Phys. Rev. Lett.* **119** no. 3, (2017) 031103, [arXiv:1612.02529](#)

- [astro-ph.CO].
- [38] E. Cotner and A. Kusenko, “Primordial black holes from scalar field evolution in the early universe,” *Phys. Rev. D* **96** no. 10, (2017) 103002, [arXiv:1706.09003 \[astro-ph.CO\]](#).
- [39] E. Cotner, A. Kusenko, and V. Takhistov, “Primordial Black Holes from Inflaton Fragmentation into Oscillons,” *Phys. Rev. D* **98** no. 8, (2018) 083513, [arXiv:1801.03321 \[astro-ph.CO\]](#).
- [40] E. Cotner, A. Kusenko, M. Sasaki, and V. Takhistov, “Analytic Description of Primordial Black Hole Formation from Scalar Field Fragmentation,” *JCAP* **10** (2019) 077, [arXiv:1907.10613 \[astro-ph.CO\]](#).
- [41] S. W. Hawking, “Black Holes From Cosmic Strings,” *Phys. Lett. B* **231** (1989) 237–239.
- [42] A. Polnarev and R. Zembowicz, “Formation of Primordial Black Holes by Cosmic Strings,” *Phys. Rev. D* **43** (1991) 1106–1109.
- [43] J. H. MacGibbon, R. H. Brandenberger, and U. F. Wichoski, “Limits on black hole formation from cosmic string loops,” *Phys. Rev. D* **57** (1998) 2158–2165, [arXiv:astro-ph/9707146](#).
- [44] R. Brandenberger, B. Cyr, and H. Jiao, “Intermediate mass black hole seeds from cosmic string loops,” *Phys. Rev. D* **104** no. 12, (2021) 123501, [arXiv:2103.14057 \[astro-ph.CO\]](#).
- [45] S. G. Rubin, M. Y. Khlopov, and A. S. Sakharov, “Primordial black holes from nonequilibrium second order phase transition,” *Grav. Cosmol.* **6** (2000) 51–58, [arXiv:hep-ph/0005271](#).
- [46] S. G. Rubin, A. S. Sakharov, and M. Y. Khlopov, “The Formation of primary galactic nuclei during phase transitions in the early universe,” *J. Exp. Theor. Phys.* **91** (2001) 921–929, [arXiv:hep-ph/0106187](#).
- [47] N. F. Bell and R. R. Volkas, “Mirror matter and primordial black holes,” *Phys. Rev. D* **59** (1999) 107301, [arXiv:astro-ph/9812301](#).
- [48] R. Allahverdi, J. Dent, and J. Osinski, “Nonthermal production of dark matter from primordial black holes,” *Phys. Rev. D* **97** no. 5, (2018) 055013, [arXiv:1711.10511 \[astro-ph.CO\]](#).
- [49] O. Lennon, J. March-Russell, R. Petrossian-Byrne, and H. Tillim, “Black Hole Genesis of Dark Matter,” *JCAP* **04** (2018) 009, [arXiv:1712.07664 \[hep-ph\]](#).
- [50] D. Hooper, G. Krnjaic, and S. D. McDermott, “Dark Radiation and Superheavy Dark Matter from Black Hole Domination,” *JHEP* **08** (2019) 001, [arXiv:1905.01301 \[hep-ph\]](#).
- [51] P. Gondolo, P. Sandick, and B. Shams Es Haghi, “Effects of primordial black holes on dark matter models,” *Phys. Rev. D* **102** no. 9, (2020) 095018, [arXiv:2009.02424 \[hep-ph\]](#).
- [52] A. Cheek, L. Heurtier, Y. F. Perez-Gonzalez, and J. Turner, “Primordial black hole evaporation and dark matter production. I. Solely Hawking radiation,” *Phys. Rev. D* **105** no. 1, (2022) 015022, [arXiv:2107.00013 \[hep-ph\]](#).
- [53] A. Cheek, L. Heurtier, Y. F. Perez-Gonzalez, and J. Turner, “Primordial black hole evaporation and dark matter production. II. Interplay with the freeze-in or freeze-out mechanism,” *Phys. Rev. D* **105** no. 1, (2022) 015023, [arXiv:2107.00016 \[hep-ph\]](#).
- [54] D. Hooper, G. Krnjaic, J. March-Russell, S. D. McDermott, and R. Petrossian-Byrne, “Hot Gravitons and Gravitational Waves From Kerr Black Holes in the Early Universe,” [arXiv:2004.00618 \[astro-ph.CO\]](#).
- [55] A. Arbey, J. Auffinger, P. Sandick, B. Shams Es Haghi, and K. Sinha, “Precision calculation of dark radiation from spinning primordial black holes and early matter-dominated eras,” *Phys. Rev. D* **103** no. 12, (2021) 123549, [arXiv:2104.04051 \[astro-ph.CO\]](#).
- [56] P. Sandick, B. S. Es Haghi, and K. Sinha, “Asymmetric reheating by primordial black holes,” *Phys. Rev. D* **104** no. 8, (2021) 083523, [arXiv:2108.08329 \[astro-ph.CO\]](#).
- [57] I. Masina, “Dark Matter and Dark Radiation from Evaporating Kerr Primordial Black Holes,” *Grav. Cosmol.* **27** no. 4, (2021) 315–330, [arXiv:2103.13825 \[gr-qc\]](#).
- [58] A. Cheek, L. Heurtier, Y. F. Perez-Gonzalez, and J. Turner, “Redshift effects in particle production from Kerr primordial black holes,” *Phys. Rev. D* **106** no. 10, (2022) 103012, [arXiv:2207.09462 \[astro-ph.CO\]](#).
- [59] F. Schiavone, D. Montanino, A. Mirizzi, and F. Capozzi, “Axion-like particles from primordial black holes shining through the Universe,” *JCAP* **08** (2021) 063, [arXiv:2107.03420 \[hep-ph\]](#).
- [60] N. Bernal, F. Hajkarim, and Y. Xu, “Axion Dark Matter in the Time of Primordial Black Holes,” *Phys. Rev. D* **104** (2021) 075007, [arXiv:2107.13575 \[hep-ph\]](#).
- [61] K. Mazde and L. Visinelli, “The Interplay between the Dark Matter Axion and Primordial Black Holes,” [arXiv:2209.14307 \[astro-ph.CO\]](#).
- [62] Y. B. Zeldovich, “Charge Asymmetry of the Universe Due to Black Hole Evaporation and Weak Interaction Asymmetry,” *Pisma Zh. Eksp. Teor. Fiz.* **24** (1976) 29–32.
- [63] B. J. Carr, “Some cosmological consequences of primordial black-hole evaporations,” *Astrophys. J.* **206** (1976) 8–25.
- [64] D. Toussaint, S. B. Treiman, F. Wilczek, and A. Zee, “Matter - Antimatter Accounting, Thermodynamics, and Black Hole Radiation,” *Phys. Rev. D* **19** (1979) 1036–1045.
- [65] M. S. Turner, “BARYON PRODUCTION BY PRIMORDIAL BLACK HOLES,” *Phys. Lett. B* **89** (1979) 155–159.
- [66] A. F. Grillo, “Primordial Black Holes and Baryon Production in Grand Unified Theories,” *Phys. Lett. B* **94** (1980) 364–366.
- [67] D. Baumann, P. J. Steinhardt, and N. Turok, “Primordial Black Hole Baryogenesis,” [arXiv:hep-th/0703250](#).
- [68] T. Fujita, M. Kawasaki, K. Harigaya, and R. Matsuda, “Baryon asymmetry, dark matter, and density perturbation from primordial black holes,” *Phys. Rev. D* **89** no. 10, (2014) 103501, [arXiv:1401.1909 \[astro-ph.CO\]](#).
- [69] A. Hook, “Baryogenesis from Hawking Radiation,” *Phys. Rev. D* **90** no. 8, (2014) 083535, [arXiv:1404.0113 \[hep-ph\]](#).
- [70] Y. Hamada and S. Iso, “Baryon asymmetry from primordial black holes,” *PTEP* **2017** no. 3, (2017) 033B02, [arXiv:1610.02586 \[hep-ph\]](#).
- [71] L. Morrison, S. Profumo, and Y. Yu, “Melanogenesis: Dark Matter of (almost) any Mass and Baryonic Matter from the Evaporation of

- Primordial Black Holes weighing a Ton (or less),” *JCAP* **05** (2019) 005, [arXiv:1812.10606 \[astro-ph.CO\]](#).
- [72] D. Hooper and G. Krnjaic, “GUT Baryogenesis With Primordial Black Holes,” *Phys. Rev. D* **103** no. 4, (2021) 043504, [arXiv:2010.01134 \[hep-ph\]](#).
- [73] N. Bernal, C. S. Fong, Y. F. Perez-Gonzalez, and J. Turner, “Rescuing high-scale leptogenesis using primordial black holes,” *Phys. Rev. D* **106** no. 3, (2022) 035019, [arXiv:2203.08823 \[hep-ph\]](#).
- [74] T. C. Gehrman, B. Shams Es Haghi, K. Sinha, and T. Xu, “Baryogenesis, Primordial Black Holes and MHz-GHz Gravitational Waves,” [arXiv:2211.08431 \[hep-ph\]](#).
- [75] S. C. Kappadath, *Measurement of the Cosmic Diffuse Gamma-Ray Spectrum from 800 KEV to 30 Mev*. PhD thesis, University of New Hampshire, United States, Jan., 1998.
- [76] Fermi-LAT Collaboration, W. B. Atwood *et al.*, “The Large Area Telescope on the Fermi Gamma-ray Space Telescope Mission,” *Astrophys. J.* **697** (2009) 1071–1102, [arXiv:0902.1089 \[astro-ph.IM\]](#).
- [77] R. D. Peccei and H. R. Quinn, “CP conservation in the presence of pseudoparticles,” *Phys. Rev. Lett.* **38** (Jun, 1977) 1440–1443. <https://link.aps.org/doi/10.1103/PhysRevLett.38.1440>.
- [78] R. D. Peccei and H. R. Quinn, “Constraints imposed by CP conservation in the presence of pseudoparticles,” *Phys. Rev. D* **16** (Sep, 1977) 1791–1797. <https://link.aps.org/doi/10.1103/PhysRevD.16.1791>.
- [79] L. Abbott and P. Sikivie, “A cosmological bound on the invisible axion,” *Physics Letters B* **120** no. 1, (1983) 133–136. <https://www.sciencedirect.com/science/article/pii/037026938390638X>.
- [80] J. Preskill, M. B. Wise, and F. Wilczek, “Cosmology of the invisible axion,” *Physics Letters B* **120** no. 1, (1983) 127–132. <https://www.sciencedirect.com/science/article/pii/0370269383906378>.
- [81] M. Dine and W. Fischler, “The not-so-harmless axion,” *Physics Letters B* **120** no. 1, (1983) 137–141. <https://www.sciencedirect.com/science/article/pii/0370269383906391>.
- [82] R. T. Co, L. J. Hall, and K. Harigaya, “QCD Axion Dark Matter with a Small Decay Constant,” *Phys. Rev. Lett.* **120** no. 21, (2018) 211602, [arXiv:1711.10486 \[hep-ph\]](#).
- [83] K. Freese, J. A. Frieman, and A. V. Olinto, “Natural inflation with pseudo - Nambu-Goldstone bosons,” *Phys. Rev. Lett.* **65** (1990) 3233–3236.
- [84] J. E. Kim, H. P. Nilles, and M. Peloso, “Completing natural inflation,” *JCAP* **01** (2005) 005, [arXiv:hep-ph/0409138](#).
- [85] E. Pajer and M. Peloso, “A review of Axion Inflation in the era of Planck,” *Class. Quant. Grav.* **30** (2013) 214002, [arXiv:1305.3557 \[hep-th\]](#).
- [86] P. W. Graham, D. E. Kaplan, and S. Rajendran, “Cosmological Relaxation of the Electroweak Scale,” *Phys. Rev. Lett.* **115** no. 22, (2015) 221801, [arXiv:1504.07551 \[hep-ph\]](#).
- [87] R. S. Gupta, Z. Komargodski, G. Perez, and L. Ubaldi, “Is the Relaxion an Axion?,” *JHEP* **02** (2016) 166, [arXiv:1509.00047 \[hep-ph\]](#).
- [88] K. Choi and S. H. Im, “Realizing the relaxion from multiple axions and its UV completion with high scale supersymmetry,” *JHEP* **01** (2016) 149, [arXiv:1511.00132 \[hep-ph\]](#).
- [89] P. Sikivie, “Invisible Axion Search Methods,” *Rev. Mod. Phys.* **93** no. 1, (2021) 015004, [arXiv:2003.02206 \[hep-ph\]](#).
- [90] M. Bauer, M. Neubert, and A. Thamm, “Collider Probes of Axion-Like Particles,” *JHEP* **12** (2017) 044, [arXiv:1708.00443 \[hep-ph\]](#).
- [91] M. Bauer, M. Heiles, M. Neubert, and A. Thamm, “Axion-Like Particles at Future Colliders,” *Eur. Phys. J. C* **79** no. 1, (2019) 74, [arXiv:1808.10323 \[hep-ph\]](#).
- [92] C. B. Adams *et al.*, “Axion Dark Matter,” in *2022 Snowmass Summer Study*. 3, 2022. [arXiv:2203.14923 \[hep-ex\]](#).
- [93] I. G. Irastorza and J. Redondo, “New experimental approaches in the search for axion-like particles,” *Prog. Part. Nucl. Phys.* **102** (2018) 89–159, [arXiv:1801.08127 \[hep-ph\]](#).
- [94] L. Di Luzio, M. Giannotti, E. Nardi, and L. Visinelli, “The landscape of QCD axion models,” *Phys. Rept.* **870** (2020) 1–117, [arXiv:2003.01100 \[hep-ph\]](#).
- [95] K. Choi, S. H. Im, and C. Sub Shin, “Recent Progress in the Physics of Axions and Axion-Like Particles,” *Ann. Rev. Nucl. Part. Sci.* **71** (2021) 225–252, [arXiv:2012.05029 \[hep-ph\]](#).
- [96] C. O’Hare, “cajohare/axionlimits: Axionlimits.” <https://cajohare.github.io/AxionLimits/>, July, 2020.
- [97] A. Ayala, I. Domínguez, M. Giannotti, A. Mirizzi, and O. Straniero, “Revisiting the bound on axion-photon coupling from Globular Clusters,” *Phys. Rev. Lett.* **113** no. 19, (2014) 191302, [arXiv:1406.6053 \[astro-ph.SR\]](#).
- [98] C. Dessert, A. J. Long, and B. R. Safdi, “No Evidence for Axions from Chandra Observation of the Magnetic White Dwarf RE J0317-853,” *Phys. Rev. Lett.* **128** no. 7, (2022) 071102, [arXiv:2104.12772 \[hep-ph\]](#).
- [99] M. J. Dolan, F. J. Hiskens, and R. R. Volkas, “Advancing globular cluster constraints on the axion-photon coupling,” *JCAP* **10** (2022) 096, [arXiv:2207.03102 \[hep-ph\]](#).
- [100] C. Dessert, D. Dunsky, and B. R. Safdi, “Upper limit on the axion-photon coupling from magnetic white dwarf polarization,” *Phys. Rev. D* **105** no. 10, (2022) 103034, [arXiv:2203.04319 \[hep-ph\]](#).
- [101] G. Lucente, P. Carezza, T. Fischer, M. Giannotti, and A. Mirizzi, “Heavy axion-like particles and core-collapse supernovae: constraints and impact on the explosion mechanism,” *JCAP* **12** (2020) 008, [arXiv:2008.04918 \[hep-ph\]](#).
- [102] W. DeRocco, S. Wegsman, B. Grefenstette, J. Huang, and K. Van Tilburg, “First Indirect Detection Constraints on Axions in the Solar Basin,” *Phys. Rev. Lett.* **129** no. 10, (2022) 101101, [arXiv:2205.05700 \[hep-ph\]](#).
- [103] N. Vinoyoles, A. Serenelli, F. L. Villante, S. Basu, J. Redondo, and J. Isern, “New axion and hidden photon constraints from a solar data global fit,” *J. Cosmology Astropart. Phys.* **2015** no. 10, (Oct., 2015) 015–015, [arXiv:1501.01639 \[astro-ph.SR\]](#).
- [104] M. J. Dolan, F. J. Hiskens, and R. R. Volkas, “Constraining axion-like particles using the white dwarf initial-final mass relation,” *JCAP* **09** (2021) 010, [arXiv:2102.00379 \[hep-ph\]](#).

- [105] F. Kling and P. Quilès, “ALP searches at the LHC: FASER as a light-shining-through-walls experiment,” *Phys. Rev. D* **106** no. 5, (2022) 055036, [arXiv:2204.03599 \[hep-ph\]](#).
- [106] Belle-II Collaboration, F. Abudinén *et al.*, “Search for Axion-Like Particles produced in e^+e^- collisions at Belle II,” *Phys. Rev. Lett.* **125** no. 16, (2020) 161806, [arXiv:2007.13071 \[hep-ex\]](#).
- [107] C. Balázs *et al.*, “Cosmological constraints on decaying axion-like particles: a global analysis,” [arXiv:2205.13549 \[astro-ph.CO\]](#).
- [108] K. Langhoff, N. J. Outmezguine, and N. L. Rodd, “Irreducible Axion Background,” *Phys. Rev. Lett.* **129** no. 24, (2022) 241101, [arXiv:2209.06216 \[hep-ph\]](#).
- [109] M. Srednicki, “Axion couplings to matter: (i). cp-conserving parts,” *Nuclear Physics B* **260** no. 3, (1985) 689–700. <https://www.sciencedirect.com/science/article/pii/0550321385900549>.
- [110] J. E. Kim and G. Carosi, “Axions and the Strong CP Problem,” *Rev. Mod. Phys.* **82** (2010) 557–602, [arXiv:0807.3125 \[hep-ph\]](#). [Erratum: *Rev.Mod.Phys.* 91, 049902 (2019)].
- [111] K. Agashe, J. H. Chang, S. J. Clark, B. Dutta, Y. Tsai, and T. Xu, “Correlating gravitational wave and gamma-ray signals from primordial black holes,” *Phys. Rev. D* **105** no. 12, (2022) 123009, [arXiv:2202.04653 \[astro-ph.CO\]](#).
- [112] P. F. Depta, M. Hufnagel, and K. Schmidt-Hoberg, “Robust cosmological constraints on axion-like particles,” *JCAP* **05** (2020) 009, [arXiv:2002.08370 \[hep-ph\]](#).
- [113] P. F. Depta, M. Hufnagel, and K. Schmidt-Hoberg, “Updated BBN constraints on electromagnetic decays of MeV-scale particles,” *JCAP* **04** (2021) 011, [arXiv:2011.06519 \[hep-ph\]](#).
- [114] A. Caputo, G. Raffelt, and E. Vitagliano, “Muonic boson limits: Supernova redux,” *Phys. Rev. D* **105** no. 3, (2022) 035022, [arXiv:2109.03244 \[hep-ph\]](#).
- [115] S. W. Hawking, “Black hole explosions,” *Nature* **248** (1974) 30–31.
- [116] D. N. Page, “Particle Emission Rates from a Black Hole: Massless Particles from an Uncharged, Nonrotating Hole,” *Phys. Rev. D* **13** (1976) 198–206.
- [117] J. H. MacGibbon and B. R. Webber, “Quark and gluon jet emission from primordial black holes: The instantaneous spectra,” *Phys. Rev. D* **41** (1990) 3052–3079.
- [118] A. Arbey and J. Auffinger, “BlackHawk: A public code for calculating the Hawking evaporation spectra of any black hole distribution,” *Eur. Phys. J. C* **79** no. 8, (2019) 693, [arXiv:1905.04268 \[gr-qc\]](#).
- [119] A. Arbey and J. Auffinger, “Physics Beyond the Standard Model with BlackHawk v2.0,” *Eur. Phys. J. C* **81** (2021) 910, [arXiv:2108.02737 \[gr-qc\]](#).
- [120] J. F. Navarro, C. S. Frenk, and S. D. M. White, “A Universal density profile from hierarchical clustering,” *Astrophys. J.* **490** (1997) 493–508, [arXiv:astro-ph/9611107](#).
- [121] P. F. de Salas, K. Malhan, K. Freese, K. Hattori, and M. Valluri, “On the estimation of the local dark matter density using the rotation curve of the Milky Way,” *J. Cosmology Astropart. Phys.* **2019** no. 10, (Oct., 2019) 037, [arXiv:1906.06133 \[astro-ph.GA\]](#).
- [122] M. M. Flores and A. Kusenko, “Primordial black holes as a dark matter candidate in theories with supersymmetry and inflation,” [arXiv:2108.08416 \[hep-ph\]](#).
- [123] T. H. Jung and T. Okui, “Primordial black holes from bubble collisions during a first-order phase transition,” [arXiv:2110.04271 \[hep-ph\]](#).
- [124] G. Cowan, K. Cranmer, E. Gross, and O. Vitells, “Asymptotic formulae for likelihood-based tests of new physics,” *Eur. Phys. J. C* **71** (2011) 1554, [arXiv:1007.1727 \[physics.data-an\]](#). [Erratum: *Eur.Phys.J.C* 73, 2501 (2013)].
- [125] W. A. Rolke, A. M. Lopez, and J. Conrad, “Limits and confidence intervals in the presence of nuisance parameters,” *Nucl. Instrum. Meth. A* **551** (2005) 493–503, [arXiv:physics/0403059](#).
- [126] T. Bringmann, X. Huang, A. Ibarra, S. Vogl, and C. Weniger, “Fermi LAT Search for Internal Bremsstrahlung Signatures from Dark Matter Annihilation,” *JCAP* **07** (2012) 054, [arXiv:1203.1312 \[hep-ph\]](#).
- [127] Fermi-LAT Collaboration, M. Ackermann *et al.*, “Updated search for spectral lines from Galactic dark matter interactions with pass 8 data from the Fermi Large Area Telescope,” *Phys. Rev. D* **91** no. 12, (2015) 122002, [arXiv:1506.00013 \[astro-ph.HE\]](#).
- [128] S. Clark, B. Dutta, Y. Gao, Y.-Z. Ma, and L. E. Strigari, “21 cm limits on decaying dark matter and primordial black holes,” *Phys. Rev. D* **98** no. 4, (2018) 043006, [arXiv:1803.09390 \[astro-ph.HE\]](#).
- [129] A. M. Green and B. J. Kavanagh, “Primordial Black Holes as a dark matter candidate,” *J. Phys. G* **48** no. 4, (2021) 043001, [arXiv:2007.10722 \[astro-ph.CO\]](#).
- [130] Y. Jho, T. G. Kim, J.-C. Park, S. C. Park, and Y. Park, “Axions from Primordial Black Holes,” to appear.